Microfluidics and Nanofluidics (2018) 22:49
https://doi.org/10.1007/s10404-018-2070-4

RESEARCH PAPER

Fluid rheological effects on particle migration in a straight rectangular microchannel

Di Li[1] · Xiangchun Xuan[1]

Received: 9 February 2018 / Accepted: 7 April 2018

Abstract
There has recently been a significantly increasing interest in the passive manipulation of particles in the flow of non-Newtonian fluids through microchannels. However, an accurate and comprehensive understanding of the various fluid rheological effects on particle migration is still largely missing. We present in this work a systematic experimental study of both the individual and the combined effects of fluid inertia, elasticity, and shear thinning on the motion of rigid spherical particles in a straight rectangular microchannel. We first study the sole effect of each of these rheological properties in a Newtonian fluid, purely elastic (i.e., Boger) fluid, and purely shear-thinning (i.e., pseudoplastic) fluid, respectively. We then study the combined effects of two or all of these rheological properties in a pseudoplastic fluid and two types of elastic shear-thinning fluids, respectively. We find that the fluid elasticity effect directs particles toward the centerline of the channel while the fluid shear-thinning effect causes particle migration toward both the centerline and corners. These two effects are combined with the fluid inertial effect to understand the particle migration in inertial pseudoplastic and viscoelastic fluid flows.

Keywords Particle migration · Shear thinning · Elasticity · Elastic lift · Inertial lift · Microfluidics

1 Introduction

Manipulating precisely the motion of particles in microchannels is important for microfluidic devices to achieve focusing (Xuan et al. 2010), trapping (Huang et al. 2017), concentration (Nilsson et al. 2009), washing (Tarn et al. 2014), and separation (Sajeesh and Sen 2014), etc., for various chemical and biological applications. It has been typically implemented by imposing a force field, such as electric (Li et al. 2014), magnetic (Hejazian et al. 2015), acoustic (Nam et al. 2011), or optical (Kayani et al. 2012) force, relative to the flow. This type of *active* methods often suffers from a relatively low throughput due to the limited action time of the external force (Karimi et al. 2013). In contrast, the *passive* control of particle motion by the use of the flow-induced lift and/or drag forces has the potential to achieve a high throughput with also the advantages of simplicity and effectiveness (Liu and Hu 2017; Yan et al. 2017). It has thus been increasingly studied in the past decade, which can take place in either a Newtonian fluid (Di Carlo 2009; Amini et al. 2014) or a non-Newtonian fluid (D'Avino and Maffettone 2015; D'Avino et al. 2017).

Fluid inertia has been demonstrated to cause a transverse migration of particles in a confined flow of Newtonian fluids (Segre and Silberberg 1961; Ho and Leal 1974; Leal 1980), yielding the so-called inertial focusing in microchannels for a variety of lab-on-a-chip applications (Martel and Toner 2014; Zhang et al. 2016). In non-Newtonian fluids, particle migration can occur even in a flow with negligible inertial effects (Karnis et al. 1963; Karnis and Mason 1966), which is attributed to an additional force arising from the gradients of normal stresses in the undisturbed flow (Ho and Leal 1976). This force is often termed viscoelastic or simply elastic lift in the microfluidics community (Liu and Hu 2017; Lu et al. 2017; Yuan et al. 2018), as distinguished from the inertial lift (Amini et al. 2014; Martel and Toner 2014; Zhang et al. 2016). The sole action of the elastic lift and mutual action of the elastic/inertial lifts on particle migration have been investigated in the flow of various polymer solutions [e.g., polyvinylpyrrolidone (PVP) (Romeo et al. 2013; Del Giudice et al. 2013; Xiang et al. 2016a), polyethylene oxide (PEO) (Lee et al. 2013; Li et al. 2016; Liu et al. 2015a; Lu and Xuan 2015; Lu et al. 2015; Xiang et al. 2016b; Yuan

✉ Di Li
xcxuan@clemson.edu

[1] Department of Mechanical Engineering, Clemson University, Clemson, SC 29634-0921, USA

Published online: 11 April 2018

et al. 2015), and polyacrylamide (PAA) (Leshansky et al. 2007; Lim et al. 2014b)] and biological fluids [e.g., hyaluronic acid (HA) (Lim et al. 2014a; Nam et al. 2015; Asghari et al. 2017) and DNA solutions (Kang et al. 2013; Kim and Kim 2016)] through different microchannels. They are found to be a strong function of fluid rheological properties including elasticity and shear thinning.

The fluid elasticity effect has been long known (Leal 1979) to direct particles toward the region of the lowest absolute shear rate, which is the centerline for a plane or cylindrical Poiseuille flow (Karnis and Mason 1966; Leshansky et al. 2007; Seo et al. 2014c) and the centerline/corners for a rectangular Poiseuille flow (Yang et al. 2012; Villone et al. 2013; Seo et al. 2014b). This migration can be significantly influenced by the fluid inertial effect (Li et al. 2015; Villone et al. 2013; Yang et al. 2011). The fluid shear-thinning effect has been demonstrated to promote the particle migration away from the channel centerline (Huang and Joseph 2000; D'Avino et al. 2012; Del Giudice et al. 2015, 2017; Liu et al. 2016; Seo et al. 2014a, b; Song et al. 2016) in confined viscoelastic flows. It becomes more pronounced as the fluid inertial and elasticity effects increase (Villone et al. 2013; Li et al. 2015). However, the sole effect of fluid shear thinning has been nearly unexplored except the work from Gauthier et al. (1971a, b). In those two studies, rigid particles were observed to migrate in the direction of maximum shear rate in a purely viscous fluid with strong shear thinning (labeled pseudoplastic) in two-dimensional Couette (Gauthier et al. 1971a) and Poiseuille (Gauthier et al. 1971b) flows, respectively. This migration was found opposite to that of particles suspended in a viscoelastic fluid.

The aim of this work is to decompose the effects of fluid rheological properties on particle migration in a straight rectangular microchannel via a systematic experimental investigation. We first study the sole effect of fluid inertia (Sect. 4.1), fluid elasticity (Sect. 4.2), and fluid shear thinning (Sect. 4.3) on the migration of rigid spherical particles in a Newtonian fluid (water), purely elastic fluid (i.e., Boger fluid (James 2009), PVP solution), and pseudoplastic fluid (xanthan solution), respectively. We then study the combined effects of two (Sect. 4.4) or all three rheological properties (Sects. 4.5 and 4.6) on the migration of the same particles in the inertial flow of pseudoplastic (xanthan solution) and elastic shear-thinning (PEO and PAA solutions) fluids, respectively. We also attempt to understand these combined fluid rheological effects using the sole effect of each property. We would like to point out that the migration of spherical particles has been well characterized in the flow of water (Sect. 4.1), PVP (Sect. 4.2), and PEO (Sect. 4.5) solutions through straight rectangular microchannels. However, to compare with the particle behaviors in xanthan (Sects. 4.3 and 4.4) and PAA (Sect. 4.6) solutions for a systematic understanding of fluid rheological effects, we carry out tests in all solutions with the same particles under identical experimental conditions.

2 Experiment

Spherical 10-μm-diameter polystyrene particles (Thermo Scientific) were used in all experiments. They were re-suspended in five types of water-based solutions with different rheological properties: (1) Newtonian fluid with a constant viscosity—water; (2) purely elastic fluid with a negligible shear-thinning effect—5% PVP solution (molecular weight, $M_w = 0.36 \times 10^6$ Da, Sigma-Aldrich); (3) pseudoplastic fluid with a strong shear-thinning effect—2000 ppm xanthan (Tokyo Chemical Industry) solution; (4) viscoelastic fluid with a weak shear-thinning effect—1000 ppm PEO solution ($M_w = 2 \times 10^6$ Da, Sigma-Aldrich); and (5) viscoelastic fluid with a strong shear-thinning effect—200 ppm PAA solution ($M_w = 18 \times 10^6$ Da, Polysciences). Each of these solutions was mixed with glycerol (Fisher Scientific) at the volume ratio of 78:22, such that polystyrene particles suspended therein become neutrally buoyant. Due to the lack of measuring equipment in our laboratory, the approximate rheological properties of these solutions were obtained from the literature (Table 1). Note that none of the polymer solutions listed in the table contains glycerol, and so the real values of the fluid viscosity and relaxation time for our prepared polymer solutions should be greater.

Figure 1a shows a picture of the rectangular microchannel, which was fabricated with polydimethylsiloxane (PDMS) using a custom-modified soft lithography technique as described elsewhere (Liang et al. 2011). The channel is 2 cm long with a measured width of 66 μm and a measured height of 54 μm. It has an expansion region at each end with an array of posts patterned therein for filtering any debris. A right-angle prism (NT 32-526, Edmund Optics Inc.) was used to visualize the particle motion in the vertical plane of the microchannel. It was embedded into the PDMS slab and placed right before the outlet expansion with a 400 μm

Table 1 Important rheological properties of the prepared solutions (without glycerol except water, estimated at 20 °C)

Solution	Polymer concentration	Relaxation time, λ (ms)	Power-law index, n	Zero shear viscosity, η_0 (mPa s)
Water[a]	0	0	1	1.86
PVP[b]	5%	2.2	~ 1	28
Xanthan[c]	2000 ppm	~ 0	0.34	3680
PEO[d]	1000 ppm	1.5	0.977	2.3
PAA[e]	200 ppm	95	0.377	22

[a]Cheng (2008); [b]Liu et al. (2015a); [c]Japper-Jaafar et al. (2010); [d]Rodd et al. (2005); [e]Poole and Escudier (2004)

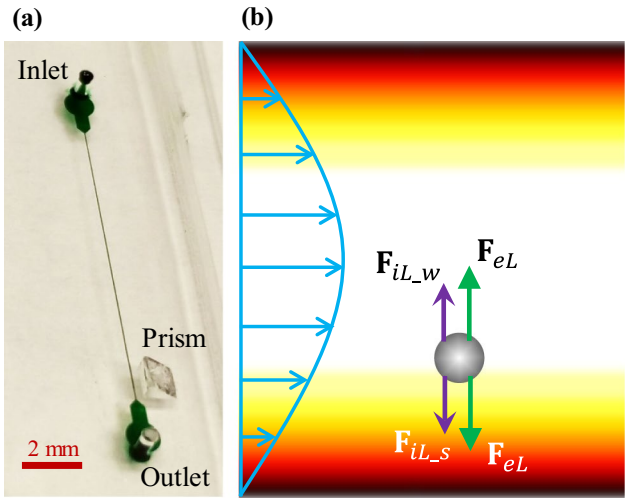

Fig. 1 **a** Picture of the straight rectangular microchannel (filled with green food dye for clarity) used in the experiment, where the right-angle prism was embedded into the PDMS slab with a 400 μm distance from the channel edge for the side viewing of particle motion. **b** Analysis of the inertial and/or elastic lift force components on a neutrally buoyant spherical particle in the flow (see the parallel arrows for the parabolic velocity profile) of Newtonian and viscoelastic fluids through a straight rectangular microchannel (see the text in Sect. 3 for the definitions of the highlighted symbols). The background color shows the contour of fluid shear rate squared, $\dot{\gamma}^2$ (the darker the larger magnitude), in the horizontal plane of the microchannel (color figure online)

distance from the microchannel edge. The prepared particle suspension was driven through the microchannel by a syringe pump (KD Scientific). Particle motion was recorded from both the top and side views with an inverted fluorescent microscope (Nikon Eclipse TE2000U, Nikon Instrument) with a CCD camera (Nikon DS-Qi1Mc). The recorded digital images were processed using the Nikon imaging software (NIS-Elements). Superimposed images were obtained by stacking a sequence of snapshot images with the maximum intensity projection.

3 Theory

Figure 1b shows the analysis of the inertial and/or elastic lift forces on particles in the flow of Newtonian and viscoelastic fluids through a straight rectangular microchannel. The inertial lift, $\mathbf{F}_{\mathrm{iL}}$, results from the inertia of the fluid and can be broken down into two components for a neutrally buoyant spherical particle, where the wall-induced lift, $\mathbf{F}_{\mathrm{iL\_w}}$, pushes the particle away from any channel walls, and the shear gradient-induced lift, $\mathbf{F}_{\mathrm{iL\_s}}$, directs the particle away from the channel centerline toward the high-shear-rate region (see the background color in Fig. 1b) (Di Carlo 2009). The following scaling formula has been often used to evaluate the inertial lift (Asmolov 1999),

$$\mathbf{F}_{\mathrm{iL}} = \mathbf{F}_{\mathrm{iL\_w}} + \mathbf{F}_{\mathrm{iL\_s}}\ \rho d^4 \dot{\gamma}^2, \tag{1}$$

where ρ is the fluid density, d is the particle diameter, and $\dot{\gamma}$ is the fluid shear rate. This force is a strong function of the Reynolds number, Re,

$$Re = \frac{\rho V D_{\mathrm{h}}}{\eta(\dot{\gamma})} = \frac{2\rho Q}{\eta(\dot{\gamma})(w+h)}, \tag{2}$$

where V is the average fluid velocity, D_{h} is the hydraulic diameter of a rectangular microchannel, $\eta(\dot{\gamma})$ is the fluid viscosity, Q is the volumetric flow rate, w is the channel width, and h is the channel height. Another dimensionless number to characterize the inertial lift is the particle Reynolds number,

$$Re_{\mathrm{p}} = Re\left(\frac{d}{D_{\mathrm{h}}}\right)^2, \tag{3}$$

which has been demonstrated to be on the order of 1 (or at least $Re_{\mathrm{p}} > 0.1$) for effective inertial focusing of particles. For shear-thinning fluids, $\eta(\dot{\gamma})$ in Eq. (2) was estimated using the Carreau–Yasuda model (Yasuda et al. 1981) at the average shear rate across the channel width, $\bar{\dot{\gamma}} = 2V/w$,

$$\frac{\eta - \eta_\infty}{\eta_0 - \eta_\infty} = \left[1 + \left(\lambda_{\mathrm{CY}}\bar{\dot{\gamma}}\right)^a\right]^{(n-1)/a}, \tag{4}$$

where η_∞ is the infinite-shear-rate viscosity, η_0 is the zero shear rate viscosity, λ_{CY} is a time constant, n is the power-law index, and a is a fitting parameter introduced by Yasuda et al. (1981). The values of the parameters in Eq. (4) (except for η_0 and n that are given in Table 1) for our prepared xanthan and PAA solutions (without glycerol) are given in Table 2. For non- and weakly shear-thinning fluids (i.e., water, PVP, and PEO solutions), $\eta(\dot{\gamma})$ was set to be η_0 in Table 1.

The elastic lift, $\mathbf{F}_{\mathrm{eL}}$, results from the non-uniform normal stress differences in non-Newtonian fluid flows (Leal 1979; D'Avino et al. 2017). Considering that the first normal stress difference often plays a dominant role in

Table 2 Parameters involved in the Carreau–Yasuda model for estimating the viscosity of the prepared xanthan and PAA solutions (without glycerol, estimated at 20 °C)

Solution	Time constant, λ_{CY} (s)	Fitting parameter, a	Infinite shear viscosity, η_∞ (mPa s)
Xanthan[a]	21.5	0.81	2.24
PAA[b]	0.551	0.623	2.62

[a]Japper-Jaafar et al. (2010); [b]Poole and Escudier (2004)

polymer solutions (Barnes et al. 1989), the elastic lift may be expressed in the following scale (Bird et al. 1977):

$$\mathbf{F}_{\mathrm{eL}} \sim d^3 \nabla \left(\Psi_1 \dot{\gamma}^2 \right), \tag{5}$$

where Ψ_1 is the first normal stress difference coefficient as a function of fluid rheological properties and shear rate. It can be characterized by the Weissenberg number, Wi, in terms of the average fluid shear rate across the channel width, $\bar{\dot{\gamma}}$,

$$Wi = \lambda \bar{\dot{\gamma}} = \lambda \frac{2V}{w} = \frac{2\lambda Q}{w^2 h}, \tag{6}$$

where λ is the fluid relaxation time. The relative contribution between $\mathbf{F}_{\mathrm{eL}}$ and $\mathbf{F}_{\mathrm{iL}}$ is dependent on the ratio of the Weissenberg number to Reynolds number, i.e., the elasticity number, El,

$$\mathrm{El} = \frac{Wi}{Re} = \frac{\lambda \eta(\dot{\gamma})(w+h)}{\rho w^2 h} \tag{7}$$

As the two lift forces are both functions of fluid rheological properties, where the most important ones are the elasticity, shear-thinning, and inertial effects [in terms of λ and $\eta(\dot{\gamma})$, respectively, in Eq. (6)], particle migration is expected to vary in different types of non-Newtonian fluids.

4 Results and discussion

4.1 Sole effect of fluid inertia

Figure 2a shows the migration of 10 μm particles in a Newtonian water/glycerol flow through a straight rectangular microchannel under the influence of fluid inertia alone. For a flow rate of up to 1 mL/h, particles are (almost) evenly distributed in both the width (see the top-view images) and depth (see the side-view images) directions of the channel due to the weak inertial lift at a very small particle Reynolds number, $Re_{\mathrm{p}} \leqslant 0.073$. As the flow rate increases to 4 mL/h, particles are observed to migrate toward two primary equilibrium positions in the channel depth direction. However, their migrations in the width direction are still not visible until the flow rate is increased to 8 mL/h due to the insufficient length of the channel. Further increasing the flow rate to 10 mL/h yields an apparent particle migration toward the channel centerline in the width direction. There exist two other focused particle streams near the walls that are not clearly seen from the top-view image because they are located at different levels from the particle stream(s) along the centerline. Figure 2b schematically illustrates these four equilibrium particle positions that are each at the center of one side (primarily two in the shorter sides of the channel) in a nearly square microchannel. Such an inertial focusing of particles in Newtonian fluid flows, as a result of the nearly symmetric distribution of shear rate in the width and depth directions (see Fig. 2c), is consistent with previous studies (Di Carlo et al. 2009; Liu et al. 2015b).

4.2 Sole effect of fluid elasticity

Figure 3a shows the migration of 10 μm particles in 5% PVP solution with the flow rate ranging from 0.1 to 10 mL/h. As the largest particle Reynolds number (at 10 mL/h) is $Re_{\mathrm{p}} = 0.048 \ll 1$, the influence of fluid inertia can be neglected and hence the particle migration is solely the result of fluid elasticity (the elasticity number is fixed at El = 36.5 due to its independence of fluid kinematics). It is important to note that the dimensionless numbers reported hereafter for polymer solutions each require a correction factor because the involving fluid properties in Tables 1 and 2 are all for glycerol-free polymer solutions only. However, this discrepancy does not change the general fluidic behavior. At the flow rate of 0.1 mL/h, particles are found to stay slightly away from the channel sidewalls in the top-view image of Fig. 3a. They, however, already exhibit an apparent migration toward the channel center in the depth direction due to the larger gradient of shear rate squared therein (Fig. 3c). With the increase in flow rate, such an elastic particle focusing effect becomes stronger due to the enhanced elastic lift in terms of the Weissenberg number, especially

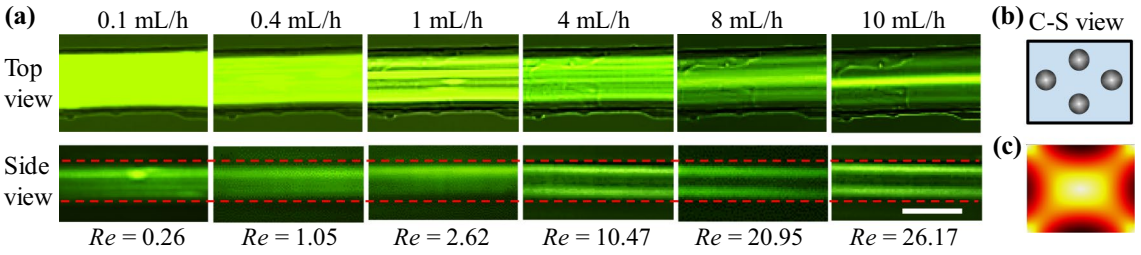

Fig. 2 Particle migration in the flow of a Newtonian water/glycerol solution through the straight rectangular microchannel: **a** top-view (upper row) and side-view (lower row) images of 10-μm-diameter particles at the channel outlet in a range of flow rates; **b** schematic of the equilibrium particle positions in the cross-sectional (C-S) view; and **c** contour of the fluid shear rate, $\dot{\gamma}$, over the channel cross section (the darker the larger magnitude). The scale bar in **a** represents 50 μm

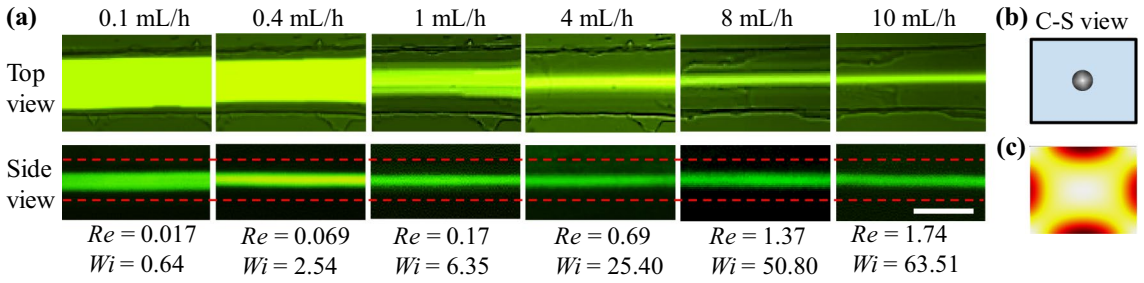

Fig. 3 Particle migration in the flow of 5% PVP solution (viscoelastic fluid with a negligible shear-thinning effect) through the straight rectangular microchannel: **a** top-view (upper row) and side-view (lower row) images of 10-μm-diameter particles at the channel outlet in a range of flow rates; **b** schematic of the equilibrium particle positions in the cross-sectional (C-S) view; and **c** contour of the fluid shear rate squared, $\dot{\gamma}^2$, over the channel cross section (the darker the larger magnitude). The scale bar in **a** represents 50 μm

significant in the channel width direction (Fig. 3a). Its equilibrium position is right at the central axis of the rectangular microchannel as schematically illustrated in Fig. 3b. This observation is consistent with earlier studies (Romeo et al. 2013; Del Giudice et al. 2013; Xiang et al. 2016a). It is, however, inconsistent with the observation of Yang et al. (2011, 2012), where near-corner motions of rigid particles were reported in an exactly square microchannel. The reason behind this discrepancy is currently unknown, which may be partially because the low-shear rate region near every corner of the channel cross section (Fig. 3c) is too small to confine 10 μm particles in our experiment due to the steric effects.

4.3 Sole effect of fluid shear thinning

Figure 4a shows the migration of 10 μm particles in the flow of pseudoplastic 2000 ppm xanthan solution through the straight rectangular microchannel. To isolate the fluid shear-thinning effect from the inertial effect, the flow rate is kept no more than 1 mL/h so that the Reynolds number is at most 0.78 (at which $Re_p = 0.022 \ll 1$). Different from those in water (Fig. 2a) and PVP solution (Fig. 3a), particles in xanthan solution (Fig. 4a) migrate toward the walls (more specifically, the corners) and centerline of the channel in both the width (top view) and depth (side view) directions in an inertialess flow. Moreover, this bidirectional particle migration is observed to increase at higher flow rates in Fig. 4a. The equilibrium positions of such a fluid shear-thinning-induced particle focusing are schematically illustrated in Fig. 3b, which should be correlated with the significantly expanded low-shear rate region over the channel cross section in a shear-thinning fluid (Fig. 3c). They seem to be qualitatively consistent with a couple of recent numerical studies that predict the fluid shear-thinning-promoted particle migration in a viscoelastic fluid toward both the corners and the centerline of a square microchannel (Li et al. 2015; Villone et al. 2013). They are also partially consistent with several other experimental and numerical studies, where the fluid shear-thinning effect has been demonstrated to weaken the elastic focusing of particles along the channel centerline in viscoelastic fluids (Huang and Joseph 2000; D'Avino et al. 2012; Del Giudice et al. 2015, 2017; Liu et al. 2016; Seo et al. 2014a, b; Song et al. 2016). More studies on particle migration in pseudoplastic fluids are needed.

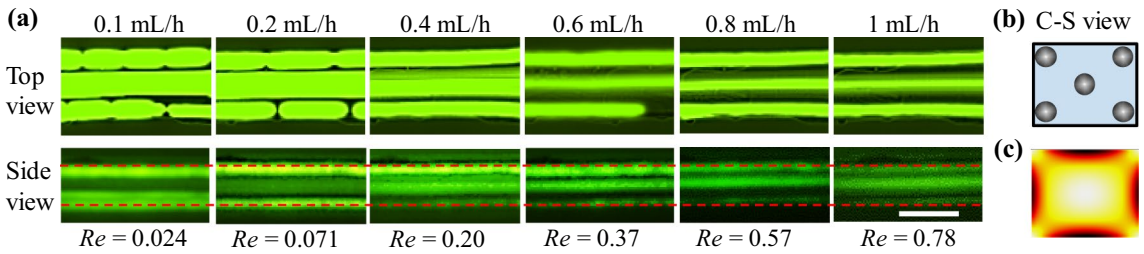

Fig. 4 Particle migration in an inertialess flow of 2000 ppm xanthan solution (pseudoplastic fluid with a strong shear-thinning effect) through the straight rectangular microchannel: **a** top-view (upper row) and side-view (lower row) images of 10-μm-diameter particles at the channel outlet in a range of flow rates from 0.1 to 1 mL/h; **b** schematic of the equilibrium particle positions in the cross-sectional (C-S) view; and **c** contour of the fluid shear rate, $\dot{\gamma}$, over the channel cross section (the darker the larger magnitude). The scale bar in **a** represents 50 μm

4.4 Combined effect of fluid shear thinning and inertia

Figure 5a shows the migration of 10 μm particles in 2000 ppm xanthan solution when the flow rate goes beyond 1 mL/h. At 2 mL/h, the Reynolds number is 1.86 and the particle Reynolds number, $Re_p = 0.052$, gets closer to 0.1. Therefore, the fluid inertia starts playing a role and, though still weak, pushing some of the particles away from the corners of channel as seen from the side-view image. This inertial effect quickly grows at 4 mL/h due to the fluid shear-thinning effect, where the Reynolds number increases to 5.07 and the particle Reynolds number, $Re_p = 0.14$, becomes greater than 0.1. As a consequence, fewer particles stay near the walls in the top-view image as compared to 2 mL/h. Moreover, the particle stream along the center of the channel in the width direction begins to split into two, which becomes more obvious at 6 mL/h. When the flow rate increases to 8 mL/h and above, we observe only two off-center particle streams in the width direction and one wide stream along the centerline in the depth direction. The equilibrium particle positions in the xanthan solution are schematically illustrated in Fig. 5b as a result of the combined action of the fluid shear-thinning-induced focusing (Fig. 4b) and the fluid inertia-induced focusing (Fig. 2b). Note that we use two nearly touching particles in the channel depth direction of the schematic in Fig. 5b to reflect the wider particle stream in the xanthan solution than that in the PVP solution (Fig. 3b).

4.5 Combined effect of fluid elasticity, weak shear thinning, and inertia

Figure 6a shows the migration of 10 μm particles in the flow of 1000 ppm PEO solution through the straight rectangular microchannel. As the PEO solution has a weak shear-thinning effect (with a power-law index of 0.977, see Table 1), the elasticity number in the range of flow rates under test remains approximately at El = 9.29. This value is only a quarter of that of 5% PVP solution (El = 36.5) (Fig. 3a), indicating a moderate elasticity in the PEO solution. It is, however, still much larger than 1, so the elastic lift should dominate the inertial lift in all flow rates (D'Avino and Maffettone 2015; D'Avino et al. 2017). As a consequence, particles already achieve an effective elastic focusing along the central axis of the channel at 0.1 mL/h ($Re = 0.21$), which is apparently better than that in the more elastic PVP solution (Fig. 3a). This is because the Weissenberg number in the PEO solution, $Wi = 1.96$, is two times greater than in the PVP solution ($Wi = 0.64$) due to the significantly lower viscosity of the former (Table 1). The effect of the weak shear thinning of the PEO solution is clearly observed at an even lower flow rate of 0.05 mL/h, where particles migrate toward both the center and corners of the channel like that in the inertialess xanthan solution (Fig. 4a).

Increasing the flow rate to 0.4 mL/h ($Re = 0.85$) causes the migration of part of the particles from the center to two symmetric off-center positions in the channel width direction due to perhaps the increased shear-thinning and inertial effects. Such a triple-stream particle focusing pattern has also been reported in previous studies (Li et al. 2016; Liu et al. 2015a; Lu et al. 2015; Xiang et al. 2016b). It quickly converts to a dual-stream pattern with the central one disappearing at 0.6 mL/h (data not shown),

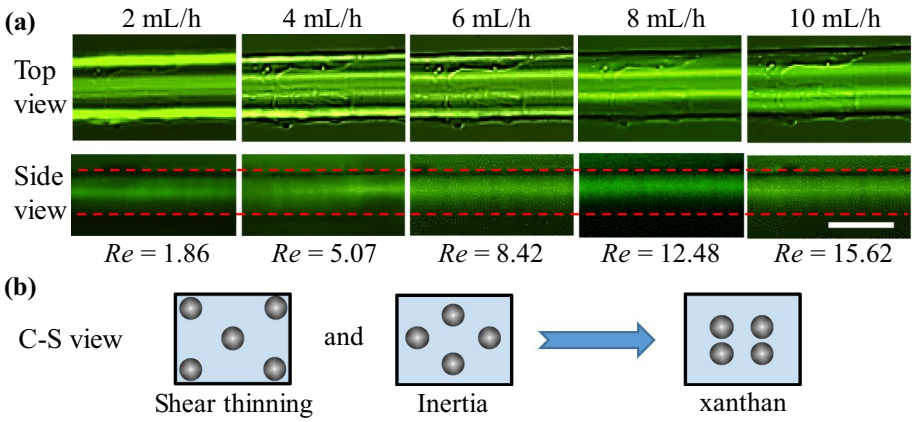

Fig. 5 Particle migration in an inertial flow of 2000 ppm xanthan solution (pseudoplastic fluid with a strong shear-thinning effect) through the straight rectangular microchannel: **a** top-view (upper row) and side-view (lower row) images of 10 μm-diameter particles at the channel outlet in a range of flow rates from 2 to 10 mL/h; **b** schematic explanation of the equilibrium particle positions in the cross-sectional (C-S) view due to the combined effects of fluid shear thinning and inertia. The scale bar in **a** represents 50 μm

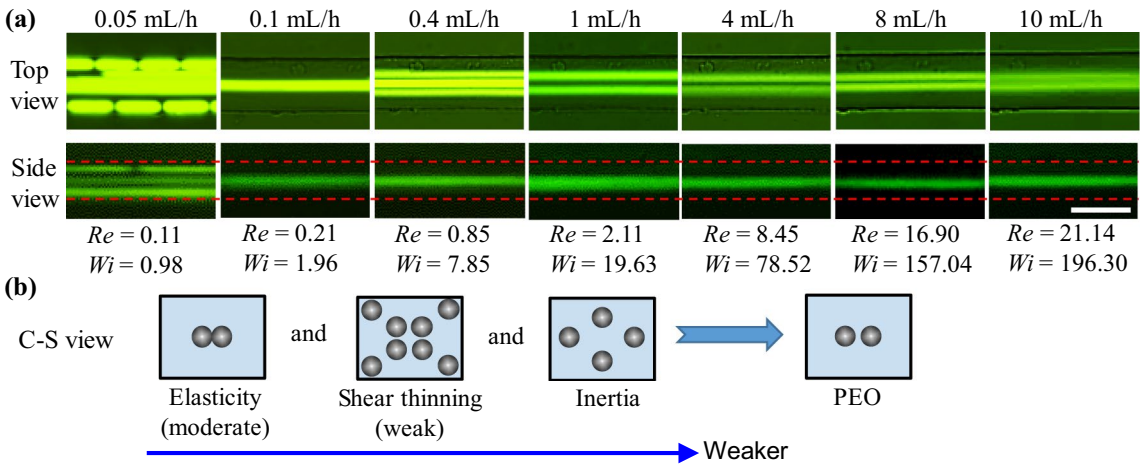

Fig. 6 Particle migration in the flow of 1000 ppm PEO solution (viscoelastic fluid with a weak shear-thinning effect) through the straight rectangular microchannel: **a** top-view (upper row) and side-view (lower row) images of 10-μm-diameter particles at the channel outlet in a range of flow rates; **b** schematic explanation of the equilibrium particle positions in the cross-sectional (C-S) view due to the combined effects of fluid elasticity, shear thinning, and inertia in the decreasing order of role (highlighted by the long arrow). The scale bar in **a** represents 50 μm

which then holds with the further increase in flow rate. However, the distance between the two streams seems to slowly decrease at higher flow rates, which is consistent with earlier studies (Li et al. 2016; Liu et al. 2015a; Lu et al. 2015; Xiang et al. 2016b) and may be a consequence of the weak fluid shear-thinning effect that increases the role of the elastic lift due to the slightly increasing elasticity number. The equilibrium particle positions in the PEO solution are schematically illustrated in Fig. 6b as a result of the combined effect of fluid elasticity (mild) (Fig. 3b), shear thinning (weak) (Fig. 4b), and inertia (Fig. 2b) in the decreasing order of role.

4.6 Combined effect of fluid elasticity, strong shear thinning, and inertia

Figure 7a shows the migration of 10 μm particles in 200 ppm PAA solution through the straight rectangular microchannel. The calculated elasticity number of this solution is El = 221.1, at 0.05 mL/h, which decreases to 151.8 at 10 mL/h due to the fluid's strong shear-thinning effect (causing a quick increase in the Reynolds number). As the lowest value of El is still significantly higher than that of PVP solution (El = 36.5), the PAA solution should be of very strong elasticity. Therefore, particles migrate toward the centerline

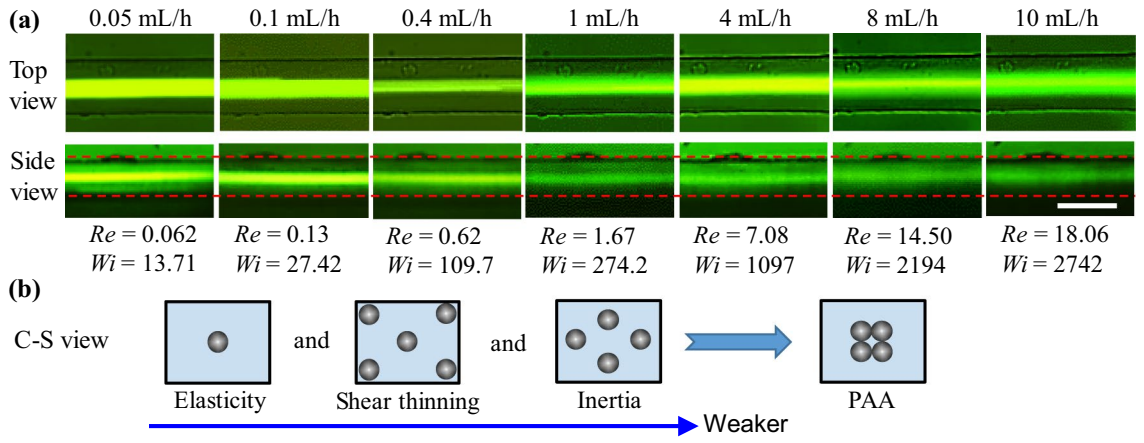

Fig. 7 Particle migration in the flow of 200 ppm PAA solution (strongly viscoelastic fluid with a strong shear-thinning effect) through the straight rectangular microchannel: **a** top-view (upper row) and side-view (lower row) images of 10-μm-diameter particles at the channel outlet in a range of flow rates; **b** schematic explanation of the equilibrium particle positions in the cross-sectional (C-S) view due to the combined effects of fluid elasticity, shear thinning, and inertia in the decreasing order of role (highlighted by the long arrow). The scale bar in **a** represents 50 μm

of the channel in both the width and depth directions even at the flow rate of 0.05 mL/h ($Re = 0.062$). No near-wall particles are observed because the fluid elasticity plays a stronger role than the fluid shear thinning. Such a single-stream particle focusing holds true in the whole range of flow rates under test. However, the particle stream width in the channel width direction seems to go through a first-decrease-then-increase trend with the increase in flow rate due to the increasing influence of fluid shear thinning and inertia. We believe it is mainly the fluid shear-thinning effect that defocuses the particles at high flow rates like that observed in the xanthan solution (Fig. 5a). The equilibrium particle positions in the PAA solution are schematically illustrated in Fig. 7b as a result of the combined effect of the strong fluid elasticity (Fig. 3b), strong fluid shear thinning (Fig. 4b), and moderate fluid inertia (Fig. 2b).

5 Conclusions

We have conducted a systematic experimental study of the migration of 10 μm polystyrene particles in the flow of five different fluids with varying rheological properties through a straight rectangular microchannel with a width/height ratio of 1.22. We find that particles migrate to four equilibrium positions in a Newtonian fluid that are each at the center of one side of the channel due to the flow-induced inertial effect. In contrast, they migrate toward the channel centerline in an elastic Boger fluid due to the fluid elasticity effect alone and toward both the centerline and corners in a pseudoplastic fluid due to the fluid shear-thinning effect alone. We have also used these individual fluid rheological effects to understand the particle motion in the inertial flow of both pseudoplastic and viscoelastic fluids. We find that particles migrate to two off-center equilibrium positions in the central plane parallel to the longer side of the channel in the pseudoplastic fluid due to the combined shear thinning and inertial effects. The addition of the fluid elasticity effect further alters the particle equilibrium position in viscoelastic fluid flows, which depends strongly on the relative significance of the three rheological effects. This developed fundamental knowledge of particle motion in the flow of various fluids will provide systematic experimental data for calibrating theoretical and numerical models, and more importantly, establish the experimental foundation for efficient *passive* manipulations (e.g., focusing and separation) of various bioparticles in non-Newtonian microfluidic devices with immediate applications to point-of-care technologies.

Acknowledgments This work was supported in part by NSF under Grant CBET-1150670 and by Clemson University through a SEED Grant.

References

Amini H, Lee W, Di Carlo D (2014) Inertial microfluidic physics. Lab Chip 14:2739–2761

Asghari M, Serhatlioglu M, Ortaç B, Solmaz ME, Elbuken C (2017) Sheathless microflow cytometry using viscoelastic fluids. Sci Rep 7:12342. https://doi.org/10.1038/s41598-017-12558-2

Asmolov ES (1999) The inertial lift on a spherical particle in a plane Poiseuille flow at large channel Reynolds number. J Fluid Mech 381:63–87

Barnes HA, Hutton JF, Walters K (1989) An introduction to rheology. Elsevier, Amsterdam

Bird RB, Armstrong RC, Hassager O (1977) Dynamics of polymeric liquids, vol 1. Wiley-Interscience, Hoboken

Cheng NS (2008) Formula for the viscosity of a glycerol–water mixture. Ind Eng Chem Res 47:3285–3288

D'Avino G, Maffettone PL (2015) Particle dynamics in viscoelastic liquids. J Non-Newton Fluid Mech 215:80–104

D'Avino G, Romeo G, Villone MM, Greco F, Netti PA, Maffettone PL (2012) Single line particle focusing induced by viscoelasticity of the suspending liquid: theory, experiments and simulations to design a micropipe flow-focuser. Lab Chip 12:1638–1645

D'Avino G, Greco F, Maffettone PL (2017) Particle migration due to viscoelasticity of the suspending liquid and its relevance in microfluidic devices. Annu Rev Fluid Mech 49:341–360

Del Giudice F, Romeo G, D'Avino G, Greco F, Netti PA, Maffettone PL (2013) Particle alignment in a viscoelastic liquid flowing in a square-shaped microchannel. Lab Chip 13:4263–4271

Del Giudice F, D'Avino G, Greco F, Netti PA, Maffettone PL (2015) Effect of fluid rheology on particle migration in a square-shaped microchannel. Microfluid Nanofluid 19:95–104

Del Giudice F, Sathish S, D'Avino G, Shen AQ (2017) "From the edge to the center": viscoelastic migration of particles and cells in a strongly shear-thinning liquid flowing in a microchannel. Anal Chem 89:13146–13159

Di Carlo D (2009) Inertial microfluidics. Lab Chip 9:3038–3046

Di Carlo D, Edd JF, Humphry KJ, Stone HA, Toner M (2009) Particle segregation and dynamics in confined flows. Phy Rev Lett 102:094503

Gauthier F, Goldsmith HL, Mason SG (1971a) Particle motions in non-Newtonian media. Rheol Acta 10:344–364

Gauthier F, Goldsmith HL, Mason SG (1971b) Particle motions in non-Newtonian media. II. Poiseuille flow. Trans Soc Rheol 15:297–330

Hejazian M, Li W, Nguyen NT (2015) Lab on a chip for continuous-flow magnetic cell separation. Lab Chip 15:959–970

Ho BP, Leal LG (1974) Inertial migration of rigid spheres in two-dimensional unidirectional flows. J Fluid Mech 65:365–400

Ho BP, Leal LG (1976) Migration of rigid spheres in a two-dimensional unidirectional shear flow of a second-order fluid. J Fluid Mech 76:783–799

Huang PY, Joseph DD (2000) Effects of shear thinning on migration of neutrally buoyant particles in pressure driven flow of Newtonian and viscoelastic fluids. J Non-Newton Fluid Mech 90:159–185

Huang L, Bian S, Cheng Y, Shi G, Liu P, Ye X, Wang W (2017) Microfluidics cell sample preparation for analysis: advances in efficient cell enrichment and precise single cell capture. Biomicrofluid 11:011501

James DF (2009) Boger fluids. Annu Rev Fluid Mech 41:129–142

Japper-Jaafar A, Escudier MP, Poole RJ (2010) Laminar, transitional and turbulent annular flow of drag-reducing polymer solutions. J Non-Newton Fluid Mech 165:1357–1372

Kang K, Lee SS, Hyun K, Lee SJ, Kim JM (2013) DNA-based highly tunable particle focuser. Nat Commun 4:2567

Karimi A, Yazdi S, Ardekani AM (2013) Hydrodynamic mechanisms of cell and particle trapping in microfluidics. Biomicrofluid 7:021501

Karnis A, Mason SG (1966) Particle motions in sheared suspensions. XIX. Viscoelastic media. Trans Soc Rheol 10:571–592

Karnis A, Goldsmith HL, Mason SG (1963) Axial migration of particles in Poiseuille flow. Nature 200:159–160

Kayani AA, Khoshmanesh K, Ward SA, Mitchell A, Kalantar-Zadeh K (2012) Optofluidics incorporating actively controlled micro- and nano-particles. Biomicrofluid 6:031501

Kim B, Kim JM (2016) Elasto-inertial particle focusing under the viscoelastic flow of DNA solution in a square channel. Biomicrofluid 10:024111

Leal LG (1979) The motion of small particles in non-Newtonian fluids. J Non-Newton Fluid Mech 5:33–78

Leal LG (1980) Particle motions in a viscous fluid. Annu Rev Fluid Mech 12:435–476

Lee DJ, Brenner H, Youn JR, Song YS (2013) Multiplex particle focusing via hydrodynamic force in viscoelastic fluids. Sci Rep 3:3258

Leshansky AM, Bransky A, Korin N, Dinnar U (2007) Tunable nonlinear viscoelastic "focusing" in a microfluidic device. Phys Rev Lett 98:234501

Li M, Li WH, Zhang J, Alici G, Wen W (2014) A review of microfabrication techniques and dielectrophoretic microdevices for particle manipulation and separation. J Phys D 47:063001

Li G, McKinley GH, Ardekani AM (2015) Dynamics of particle migration in channel flow of viscoelastic fluids. J Fluid Mech 785:486–505

Li D, Lu X, Xuan X (2016) Viscoelastic separation of particles by size in straight rectangular microchannels: a parametric study for a refined understanding. Anal Chem 88:12303–12309

Liang L, Zhu J, Xuan X (2011) Three-dimensional diamagnetic particle deflection in ferrofluid microchannel flows. Biomicrofluid 5:034110

Lim EJ, Ober TJ, Edd JF, Desai SP, Neal D, Bong KW, Doyle PS, McKinley GH, Toner M (2014a) Inertio-elastic focusing of bioparticles in microchannels at high throughput. Nat Commun 5:4120

Lim H, Nam J, Shin S (2014b) Lateral migration of particles suspended in viscoelastic fluids in a microchannel flow. Microfluid Nanofluid 17:683–692

Liu C, Hu G (2017) High-throughput particle manipulation based on hydrodynamic effects in microchannels. Micromachines 8:73

Liu C, Xue C, Chen X, Shan L, Tian Y, Hu G (2015a) Size-based separation of particles and cells utilizing viscoelastic effects in straight microchannels. Anal Chem 87:6041–6048

Liu C, Hu G, Jiang X, Sun J (2015b) Inertial focusing of spherical particles in rectangular microchannels over a wide range of Reynolds numbers. Lab Chip 15:1168–1177

Liu C, Ding B, Xue C, Tian Y, Hu G, Sun J (2016) Sheathless focusing and separation of diverse nanoparticles in viscoelastic solutions with minimized shear thinning. Anal Chem 88:12547–12553

Lu X, Xuan X (2015) Continuous microfluidic particle separation via elasto-inertial pinched flow fractionation. Anal Chem 87:6389–6396

Lu X, Zhu L, Hua RM, Xuan X (2015) Continuous sheath-free separation of particles by shape in viscoelastic fluids. Appl Phys Lett 107:264102

Lu X, Liu C, Hu G, Xuan X (2017) Particle manipulations in non-Newtonian microfluidics: a review. J Colloid Interface Sci 500:182–201

Martel JM, Toner M (2014) Inertial focusing in microfluidics. Annu Rev Biomed Eng 16:371–396

Nam J, Lee Y, Shin S (2011) Size-dependent microparticles separation through standing surface acoustic waves. Microfluid Nanofluid 11:317–326

Nam J, Tan JK, Khoo BL, Namgung B, Leo HL, Lim CT, Kim S (2015) Hybrid capillary-inserted microfluidic device for sheathless particle focusing and separation in viscoelastic flow. Biomicrofluid 9:064117

Nilsson J, Evander M, Hammarstrom B, Laurell T (2009) Review of cell and particle trapping in microfluidic systems. Anal Chim Acta 649:141–157

Poole RJ, Escudier MP (2004) Turbulent flow of viscoelastic liquids through an axisymmetric sudden expansion. J Non-Newton Fluid Mech 117:25–46

Rodd LE, Scott TP, Boger DV, Cooper-White JJ, McKinley GH (2005) The inertio-elastic planar entry flow of low-viscosity elastic fluids in micro-fabricated geometries. J Non-Newton Fluid Mech 129:1–22

Romeo G, D'Avino G, Greco F, Netti PA, Maffettone PL (2013) Viscoelastic flow-focusing in microchannels: scaling properties of the particle radial distributions. Lab Chip 13:2802–2807

Sajeesh P, Sen AK (2014) Particle separation and sorting in microfluidic devices: a review. Microfluid Nanofluid 17:1–52

Segre G, Silberberg A (1961) Radial particle displacements in Poiseuille flow of suspensions. Nature 189:209–210

Seo KW, Byeon HJ, Huh HK, Lee SJ (2014a) Particle migration and single-line particle focusing in microscale pipe flow of viscoelastic fluids. RSC Adv 4:3512–3520

Seo KW, Kang YJ, Lee SJ (2014b) Lateral migration and focusing of microspheres in a microchannel flow of viscoelastic fluids. Phys Fluids 26:063301

Seo KW, Ha YR, Lee SJ (2014c) Vertical focusing and cell ordering in a microchannel via viscoelasticity: applications for cell monitoring using a digital holographic microscopy. Appl Phys Lett 104:213702

Song HY, Lee SH, Salehiyan R, Hyun K (2016) Relationship between particle focusing and dimensionless numbers in elasto-inertial focusing. Rheol Acta 55:889–900

Tarn MD, Lopez-Martinez MJ, Pamme N (2014) On-chip processing of particles and cells via multilaminar flow streams. Anal Bioanal Chem 406:139–161

Villone MM, D'Avino G, Hulsen MA, Greco F, Maffettone PL (2013) Particle motion in square channel flow of a viscoelastic liquid: migration vs. secondary flows. J Non-Newton Fluid Mech 195:1–8

Xiang N, Dai Q, Ni Z (2016a) Multi-train elasto-inertial particle focusing in straight microfluidic channels. Appl Phys Lett 109:134101

Xiang N, Zhang X, Dai Q, Cheng J, Chen K, Ni Z (2016b) Fundamentals of elasto-inertial particle focusing in curved microfluidic channels. Lab Chip 16:2626–2635

Xuan X, Zhu J, Church C (2010) Particle focusing in microfluidic devices. Microfluid Nanofluid 9:1–16

Yan S, Zhang J, Yuan D, Li W (2017) Hybrid microfluidics combined with active and passive approaches for continuous cell separation. Electrophoresis 38:238–249

Yang S, Kim JY, Lee SJ, Lee SS, Kim JM (2011) Sheathless elasto-inertial particle focusing and continuous separation in a straight rectangular microchannel. Lab Chip 11:266–273

Yang S, Lee SS, Ahn SW, Kang K, Shim W, Lee G, Hyun K, Kim JM (2012) Deformability-selective particle entrainment and separation in a rectangular microchannel using medium viscoelasticity. Soft Matter 8:5011–5019

Yasuda K, Armstrong RC, Cohen RE (1981) Shear flow properties of concentrated solutions of linear and star branched polystyrenes. Rheol Acta 20:163–178

Yuan D, Zhang J, Yan S, Pan C, Alici G, Nguyen NT, Li W (2015) Dean-flow-coupled elasto-inertial three-dimensional particle focusing under viscoelastic flow in a straight channel with asymmetrical expansion–contraction cavity arrays. Biomicrofluid 9:044108

Yuan D, Zhao Q, Yan S, Tang SY, Alici G, Zhang J, Li W (2018) Recent progress of particle migration in viscoelastic fluids. Lab Chip. https://doi.org/10.1039/C7LC01076A

Zhang J, Yan S, Yuan D, Alici G, Nguyen NT, Warkiani ME, Li W (2016) Fundamentals and applications of inertial microfluidics: a review. Lab Chip 16:10–34